NURETH14-044

A MECHANISTIC MODEL FOR DROPLET DEPOSITION HEAT TRANSFER IN DISPERSED FLOW FILM BOILING

M. J. Meholic¹, D. L. Aumiller² and F. B. Cheung¹

¹ The Pennsylvania State University, Department of Mechanical and Nuclear Engineering,
University Park, Pennsylvania, United States

² Bettis Atomic Power Laboratory, West Mifflin, Pennsylvania, United States

<u>michael.meholic.contractor@unnpp.gov</u>, <u>david.aumiller.contractor@unnpp.gov</u>, <u>fxc4@psu.edu</u>

Abstract

A mechanistic droplet deposition model has been developed to quantify the direct contact heat transfer present in dispersed flow film boiling. Lagrangian subscale trajectory calculations utilizing realistic velocity and temperature distributions in the momentum boundary layer are used to determine the number of dispersed droplets able to achieve contact with the heated wall. Coupling the droplet deposition model with a physical direct contact heat transfer coefficient model allows the total direct contact heat transfer to be determined based upon the local vapor mass flux, wall superheat, and vapor superheat. Comparisons to the existing models highlight the more mechanistic nature of the proposed model.

1. Introduction

Film boiling heat transfer is an important phenomenon in cryogenics, once-through steam generators, and the safety analysis of nuclear power plant transients, especially for the postulated Loss-of-Coolant-Accident (LOCA). As a post-critical heat flux heat transfer regime in which the minimum film boiling temperature has been exceeded, film boiling is characterized by a continuous vapor contact with the heated surface and vapor generation at the liquid-vapor interface. Film boiling is commonly subdivided into two regimes: Inverted Annular Film Boiling (IAFB) and Dispersed Flow Film Boiling (DFFB). In IAFB, a thin vapor layer surrounds the heated surface and separates it from the liquid core. Conversely, DFFB is characterized by a continuous vapor field with dispersed droplets of saturated liquid.

The DFFB heat transfer regime can be encountered twice during the LOCA scenario and plays a vital role in accurately predicting the resulting temperatures. In the blowdown phase as the reactor depressurizes, the coolant in the reactor flashes creating a high void fraction mixture. DFFB has been found to be responsible for the cooling during blowdown which provides the initial conditions for the remainder of the transient. An accurate prediction of the DFFB heat transfer during blowdown is required to obtain the temperature distribution at the beginning of reflood. DFFB heat transfer is also responsible for the cooling of the fuel above the quench front during reflood.

Due to the importance of DFFB heat transfer, numerous correlative, phenomenological, and mechanistic DFFB models have been published. However, most of these models make inappropriate simplifying assumptions or are too computationally intensive to implement into current reactor safety codes. The objective of the current study is the development of a mechanistic, physically based modeling package which is valid over a wide range of conditions.

Due to the varying amounts of mechanical and thermal non-equilibrium present in DFFB, the contributions from the possible convective, radiative, and direct contact heat transfer paths are dependent upon the local conditions. In this work, specific attention was focused on the direct contact heat transfer component in order to accurately determine its contribution and is the topic of this paper.

2. Background

2.1 Previous Direct Contact Models

Much of the early research on DFFB was conducted at the Heat and Mass Transfer Laboratory at the Massachusetts Institute of Technology (MIT) in the 1960s. Forslund and Rohsenow [1] were the first to model direct contact, or Leidenfrost, heat transfer explicitly. Utilizing a droplet heat transfer coefficient developed by Baumeister *et al.* [2] and the number of droplets incident on the heated surface (or wall), Forslund and Rohsenow give the direct contact heat flux as:

$$q''_{wd,dc} = K_1 K_2 \left(\frac{\pi}{4}\right) \left(\frac{6}{\pi}\right)^{\frac{3}{4}} (1 - \alpha_v)^{\frac{2}{3}} \left[\frac{\tilde{\kappa}^3 H_{fg}^* g \rho_v \rho_l (T_w - T_{sat})^3}{\tilde{\mu} a}\right]^{\frac{1}{4}}$$
(1)

Forslund and Rohsenow suggest a value of 0.2 for the K_1K_2 product to account for various effects including the use of a horizontal plate heat transfer coefficient in a vertical analysis, the packing of droplets, and the influence of the heated surface on the droplets.

Iloeje *et al.* [3] extended upon the early work at MIT by devising a model that accounts for the fraction of droplets coming into contact with the wall and the fraction that enter the boundary layer and do not come into contact with the wall. Ganic and Rohsenow [4] continued the work by utilizing a two-dimensional force balance in the laminar sublayer region to determine the fraction of droplets able to contact the wall rather than the empirical relationship used by Iloeje *et al.* [3]. Moose and Ganic [5] also modelled the direct contact component. In an attempt to account for the decreasing direct contact heat transfer as the wall temperature is increased, their model is given as:

$$q''_{wd} = V_d (1 - \alpha_v) \rho_l \left[H_{fg} + C_{p,v} (T_v - T_{sat}) \right] f \left\{ 8.44 \times 10^{-4} \left(\frac{\rho_l^2 V_d^2 \overline{a}}{\rho_v \sigma} \right)^{0.341} \exp \left[1 - \left(\frac{T_w}{T_{sat}} \right)^2 \right] \right\}$$
(2)

More recent DFFB direct contact models are given by Andreani and Yadigaroglu [6] and Guo and Mishima [7]. Andreani and Yadigaroglu utilized a Lagrangian approach to determine droplet trajectories in DFFB and an Eulerian vapor temperature mesh to determine the total DFFB heat transfer including the direct contact component. The resulting model is highly mathematical, making it cumbersome to implement and computationally expensive. Guo and Mishima developed a mechanistic direct contact model accounting for the "dry contact" between the droplets and the wall. Their model is given as:

$$q''_{wd,dc} = (T_w - T_{sat}) \left[\frac{18k_v t_R^3 \rho_v (H_v - H_f) \dot{m}_D^5}{a^5 \rho_l^4 \mu_v (1 - \alpha_v) (T_w - T_{sat})} \right]^{\frac{1}{4}}$$
(3)

2.2 Deficiencies in Previous Direct Contact Models

The most commonly implemented direct contact model in the nuclear industry is a version of the Forslund and Rohsenow [1] model. However, several of the models suggested by Forslund and Rohsenow are either inapplicable for nuclear reactors or do not provide an accurate physical representation of the true situation. Lane *et al.* [8] provides a critical review of the Forslund and Rohsenow model and highlights several deficiencies in the model. One of the largest deficiencies found in Forslund and Rohsenow arises from the application of the droplet heat transfer coefficient given by Baumeister [2]. The expression was originally derived for a single droplet impacting a horizontal heated plate in a gravity field. Thus, its application to vertical flow is unphysical due to the gravitational term forcing the droplet towards the heated surface. Additional concerns arise in the use of the K_1K_2 factor which is independent of the local flow conditions. Given that turbulent fluctuations in the flow are the dominant mechanism forcing droplets towards the wall in vertical flow, as the Reynolds number (and turbulence) increases, more droplets should be forced towards the wall. Bajorek and Young [9] addressed the deficit by suggesting a Reynolds number dependent K_1K_2 factor.

$$K_1 K_2 = \max \begin{bmatrix} 0.0 \\ \min \begin{bmatrix} \frac{\text{Re}_v - 4000}{10000} \end{bmatrix}^{0.6} \\ 1.0 \end{bmatrix}$$
 (4)

The use of the Bajorek and Young effectiveness expression helps to account for the turbulence in the flow but does not remove the gravitational dependence of the model.

Furthermore, the Forslund and Rohsenow direct contact model is unphysical with respect to the wall superheat. Their model only predicts increased direct contact heat transfer as the wall superheat increases. Physically, the direct contact heat transfer term should reach a peak at a given wall superheat and then decrease back to zero when the wall superheat is significantly high enough to prevent any droplet contact. In general, the currently available direct contact heat transfer models are either too simplified to accurately predict DFFB heat transfer over a wide range of conditions or are too computationally intensive to implement into nuclear reactor safety analysis codes.

3. New Mechanistic Droplet Deposition Heat Transfer Model

The direct contact heat transfer is calculated in steps. First, the mass flux of droplets towards the wall for a given diameter droplet is determined. Next, the trajectory of droplets are calculated to determine if contact with the heated wall is possible for the given size droplet. The mass flux of droplets that contact the wall is then multiplied by a direct contact heat transfer coefficient to quantify the direct contact heat transfer. A detailed explanation of these steps follows.

3.1 Droplet Deposition Flux

To account for the various droplet sizes present in DFFB, a droplet size probability distribution function was utilized [3].

$$P(a) = 4\frac{a}{\overline{a}^2} \exp\left[-2\left(\frac{a}{\overline{a}}\right)^2\right]$$
 (5)

The maximum droplet size was determined assuming a critical droplet Weber number of 7.5 [1]. In the course of the calculations, the droplet size distribution was discretized into bins of equal total droplet volume, each with its own characteristic diameter. The trajectory corresponding to the characteristic diameter of each bin was calculated to determine if direct contact with the wall was possible for all of the droplets in the respective bin. The total droplet mass flux from the core of the flow to the wall for bins in which contact was possible was calculated using the deposition model of Yang and Lee [10]. The deposition model which is based upon the eddy diffusivity of droplets and the droplet concentration gradient accounts for the turbulence in the vapor flow by determining the average turbulent energy across the spectrum and the fluctuations in the velocities at the edge of the boundary layer.

3.2 Droplet Trajectory Model

The fraction of dispersed droplets capable of contacting the heated wall is determined using a first-principles approach similar to that applied by Ganic [4]. A two-dimensional force balance is utilized to determine the trajectory of a given droplet in the vicinity of the heated wall. For this analysis, the axial direction is taken as the x-direction and positive in the upward flow direction. The y-direction (transverse) is normal to the heated surface and taken as zero at the wall. The position of the center of the droplet is denoted as (x,y).

Assuming an incompressible flow, the forces acting upon droplets in the momentum boundary layer are the drag force, body force, lift forces, and a differential evaporation (or thrust) force. The thrust force term is applicable in the transverse direction and is a result of vapor temperature gradient present in the boundary layer which evaporates the side of the droplet near the wall slightly more than the opposite side of the droplet. This differential evaporation causes a pressure gradient across the droplet which acts to repel the droplet away from the wall and prevent deposition. The Lee and Almenas [11] model was selected for the thrust force as it allows for any boundary layer temperature profile to be modeled. Their thrust force is given as:

$$\vec{F}_{DE} = \left\langle v_{vap} \right\rangle \frac{h_{vd}}{H_{fg}} \frac{\pi}{8} a^3 \frac{dT}{dy} \tag{6}$$

The axial droplet force balance is given as:

$$\frac{\pi}{6}\rho_l a^3 \frac{d^2 x}{dt^2} = \frac{\pi}{16}\rho_v a^3 \frac{dU}{dy} \left(\frac{dy}{dt}\right) - \frac{\pi}{8}\rho_v a^2 C_D \left(\frac{dx}{dt} - U\right) \left|\frac{dx}{dt} - U\right| - \frac{\pi}{6}(\rho_l - \rho_v) a^3 g \tag{7}$$

Equation 7 gives the change in axial momentum to be equal to the sum of the axial lift force, the axial drag force, and the axial body force terms. In the transverse direction, the droplet force balance is given as:

$$\frac{\pi}{6}\rho_{l}a^{3}\frac{d^{2}y}{dt^{2}} = -\frac{\pi}{16}\rho_{v}a^{3}\frac{dU}{dy}\left(\frac{dx}{dt} - U\right) - \frac{\pi}{8}\rho_{v}a^{2}C_{D}\left(\frac{dy}{dt}\right)\left|\frac{dy}{dt}\right| + \left\langle v_{vap}\right\rangle \frac{h_{vd}}{H_{fg}}\frac{\pi}{8}a^{3}\frac{dT}{dy}$$
(8)

Equation 8 gives the change in the transverse momentum to be equal to the sum of the transverse lift force, the transverse drag force, and the transverse differential evaporation force terms. The initial conditions used to solve the trajectory equations were:

$$t = 0, x = 0, \frac{dx}{dt} = u_0$$

$$t = 0, y = \delta, \frac{dy}{dt} = -v_0$$
(9)

The initial axial velocity of the droplet is calculated from a force balance on the droplet. The initial transverse velocity is calculated from the deposition velocity model of Liu and Ilori [12]. Utilizing this approach, the initial droplet velocity is dependent upon the mainstream velocity linking the wall droplet deposition to the mainstream turbulence and the droplet diameter. Assuming turbulent vapor flow and a boundary layer thickness of $y^+ = 30$ as suggested by Schlichting [13], the universal velocity profile can be utilized to characterize the bulk vapor velocity in the boundary layer.

$$U(y) = \begin{cases} \frac{yu^{*^{2}}}{v}, & 5\frac{v}{u^{*}} < y\\ -3.05u^{*} + 5.0u^{*} \ln\left(\frac{yu^{*}}{v}\right), & 5\frac{v}{u^{*}} \le y < 30\frac{v}{u^{*}} \end{cases}$$
(10)

Similarly, if a Prandtl number of unity is assumed, the bulk vapor temperature profile can be formulated from the universal velocity profile.

$$T(y) = (T_{v} - T_{w}) \frac{U(y)}{U_{\infty}} + T_{w}$$
(11)

The velocity profile, velocity gradient, and temperature gradients can be substituted into the trajectory equations to calculate the droplet trajectory. The trajectory equations are then solved numerically utilizing a finite difference methodology. During the course of the calculation, the droplet diameter was updated to account for its evaporation as it traversed the boundary layer. The droplet drag coefficient was also updated throughout the calculation. The drag coefficient for a sphere given by Clift and Gauvin [14] was utilized accounting for the blowing effect caused by the evaporation.

$$C_D^i = \frac{\frac{24}{\text{Re}_a^i} \left(1.0 + 0.15 \,\text{Re}_a^{i 0.687} \right) + \frac{0.42}{1 + 4.25 \times 10^4 \,\text{Re}_a^{i - 1.16}}}{1 + \frac{C_{p,v} \left(T^i - T_{sat} \right)}{H_{fg}}}$$
(12)

The interfacial heat transfer in the boundary layer is modeled using the correlation of Beard and Pruppacher [15].

$$Nu_a = 1.56 + 0.616 \text{Re}_a^{0.5} \text{Pr}_v^{0.33}$$
 (13)

3.3 Droplet Force Balances

With the force balances and the constitutive relationships, the forces acting upon a droplet can be calculated given its diameter, the local pressure, mass flux, bulk vapor temperature, and the wall temperature. The top plot of Figure 1 depicts the transverse forces acting on a 50 micron droplet with a wall superheat of 300 K. The thrust force increases as the droplet moves closer towards the wall and the local temperature gradient increases. The thrust force continues to increase until the droplet trajectory is reversed and the droplet begins to move back towards the core of the flow. The thrust force reaches a minimum in this case at approximately 0.011 seconds after the droplet enters the boundary layer when the relative velocity between the droplet and the vapor reaches zero and the droplet Reynolds number goes to zero. The thrust term then increases again as a relative velocity is once again present.

The lift force is initially negative in this case, pulling the droplet towards the heated wall since the droplet velocity is initially greater than the local vapor velocity. As the droplet is slowed by the drag and thrust forces, the lift force becomes less negative before becoming positive when the relative velocity between the droplet and local vapor changes sign. Compared to the thrust and lift forces, the drag force is very small on the 50 micron droplet. The drag force is always opposes the direction of motion as long as a relative velocity is present. Overall, the sum of the forces is positive causing the droplet to be pushed away from the wall. Once the initial inertia of the droplet has been expended, the net forces act to push the droplet back into the bulk flow.

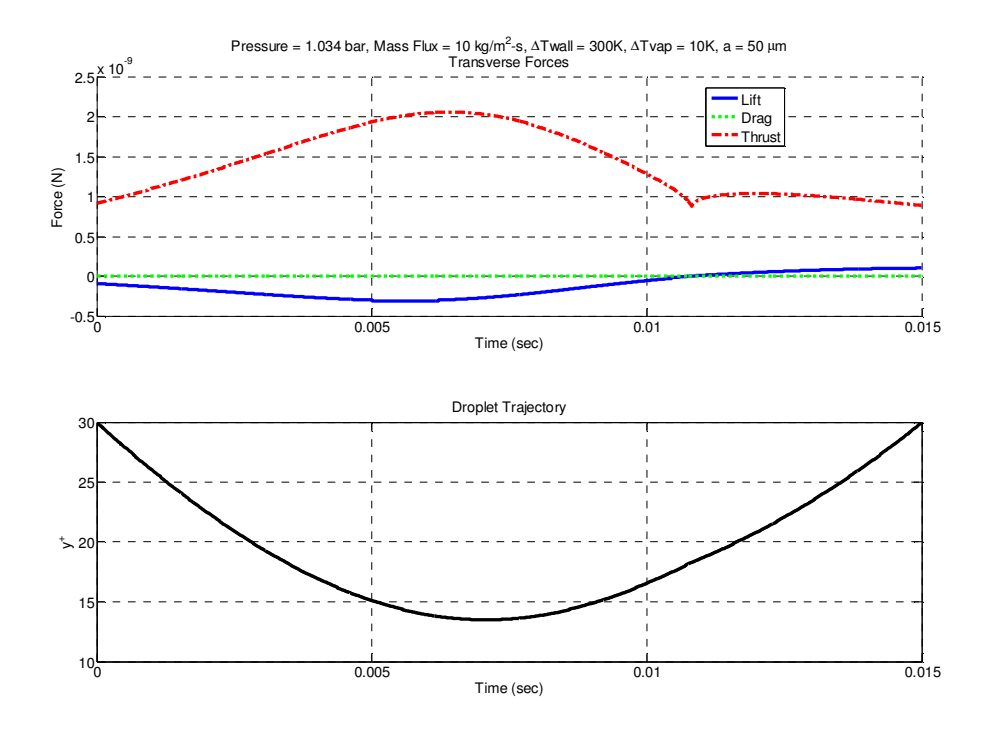


Figure 1: Transverse Forces and Trajectory for a Repelled Droplet

3.4 Droplet Trajectory Sensitivity Analysis

The droplet trajectory sensitivities to the input parameters are illustrated in Figure 2. As the upper left plot in Figure 2 illustrates, larger droplets are able to traverse further into the boundary layer than smaller droplets due to their larger initial momentum. The upper right plot in Figure 2

shows the sensitivity to the mass flux. As the mass flux increases, the droplets are imparted a greater initial transverse velocity and inertia. For the lower mass fluxes of 10 and 15 kg/m 2 -s, the droplet does not have sufficient inertia to overcome the repulsive forces. As the mass flux (and initial transverse velocity) is increased to 20 and 25 kg/m 2 -s, the droplet is able to overcome the repulsive forces and achieve contact with the wall.

In the lower left plot of Figure 2, the wall superheat sensitivity is shown. The trajectories change as a result of the varying thrust force. The thrust force overcomes the initial droplet inertia and returns it to the bulk flow for the wall superheats of 300 K and 400 K whereas for the lower superheats, contact is achieved. The sensitivity to the vapor superheat is shown in the lower right plot of Figure 2. The effect of varying the repulsion force can also be seen by changing the vapor superheat. As the vapor superheat increases, the temperature gradient across the boundary layer is decreased yielding lower thrust forces. The trajectory is also sensitive to the local pressure. Contact with the wall tends to be achieved more readily for lower pressures as a result of property changes (especially the change in the latent heat of vaporization in the thrust force).

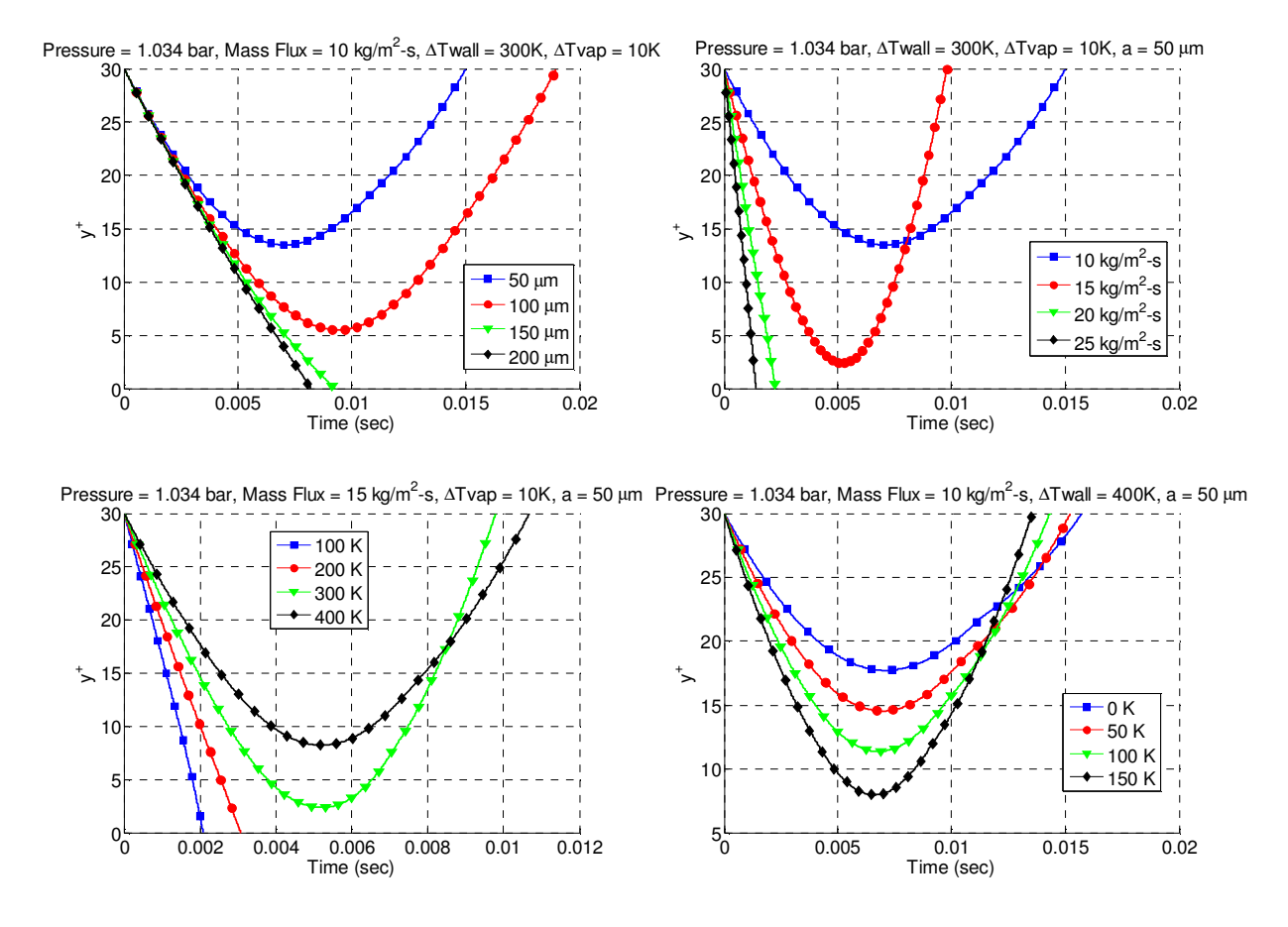


Figure 2: Droplet Trajectory Sensitivity Analysis

3.5 Direct Contact Heat Transfer Coefficient

The total heat transferred from the heated surface to the droplets which come into contact with the wall can be calculated as the number of droplets contacting the wall times the heat transferred to a single droplet, $Q_{\rm sd}$.

The 14th International Topical Meeting on Nuclear Reactor Thermal Hydraulics, NURETH-14 Toronto, Ontario, Canada, September 25-30, 2011

$$q_{wd,dc}''' = \frac{\dot{m}_D}{\frac{\pi}{6}\rho_l a^3} Q_{sd} \tag{14}$$

As a droplet "contacts" the wall, a thin vapor film forms between the liquid droplet and the heated wall resulting in "dry" contact. During the impinging process, the droplets will flatten out before recovering their spherical shape. Rayleigh studied the droplet deformation process and gives the droplet base diameter [16]:

$$\left(\frac{a_b}{a}\right)^2 = 6.97 \left[\left(\frac{t}{t_R}\right) - \left(\frac{t}{t_R}\right)^2 \right] \tag{15}$$

where the residence time (time in which the droplet is in contact with the wall) is expressed as [16]:

$$t_R = \pi \sqrt{\frac{\rho_l a^3}{16\sigma}} \tag{16}$$

Guo and Mishima [7] derived an expression for the heat transferred to a single droplet making dry contact with the heated wall using the residence time of Rayleigh. Their formulation utilizes a Navier Stokes approach in the vapor film to formulate vapor momentum, mass velocity, mass balance, and pressure equations to determine the heat transferred to a single drop.

$$Q_{sd} = \frac{\pi}{4} k_{v} (T_{w} - T_{sat}) a^{2} t_{R} \left[\frac{32 \rho_{l} \rho_{v} H_{fg}^{*} v_{o}}{9 k_{v} \mu_{v} (T_{w} - T_{sat}) t_{R} a} \right]^{\frac{1}{4}}$$
(17)

Thus, the heat flux resulting from direct contact can be determined by substituting Equation 17 into Equation 14.

4. Comparison to Previous Models

The proposed direct contact model was compared to previous models including the models of Forslund-Rohsenow [1] and Bajorek-Young [9] for a given set of conditions. The limitations and advantages of the various models can be illustrated in the results. Figure 3 compares Forslund-Rohsenow and Bajorek-Young to the current model as a function of wall superheat. Both Forslund-Rohsenow and Bajorek-Young continue to increase as the wall superheat increases. However as the wall superheat increases, the number of droplets physically able to contact the wall should decrease due to the increasing differential evaporation. The balance of the increasing temperature difference and the decreasing number of droplets able to contact the wall superheat increases is illustrated in the current model. For wall superheats up to approximately 450 K for the given conditions, the increased temperature difference increases the direct contact heat transfer. For superheats greater than 450 K at the given conditions, the number of droplets able to contact the wall begins to decrease causing the decline in the direct contact heat transfer.

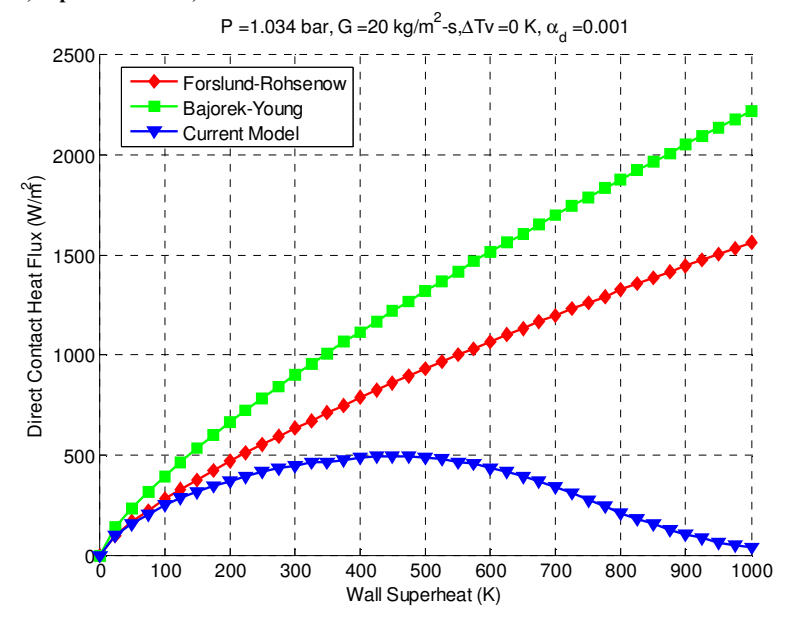


Figure 3: Comparison of Direct Contact Heat Transfer Models for Various Wall Superheats

Figure 4 compares the direct contact models as a function of the vapor mass flux. As previously mentioned, the Forslund-Rohsenow model is independent of the vapor mass flux predicting the same direct contact heat transfer regardless of the vapor mass flux. The Bajorek-Young model addressed this concern with the Forslund-Rohsenow model. For the given conditions, the Bajorek-Young model predicts direct contact heat transfer begins when the vapor mass flux exceeds 4 kg/m^2 -s (corresponding to a vapor Reynolds number of approximately 4,000). The effect of the Reynolds number dependent K_1K_2 coefficient is also seen in Figure 4 as the direct contact heat transfer increases with the increasing vapor mass flux. With the current model, direct contact heat transfer is found to start when the vapor mass flux exceeds 12 kg/m^2 -s.

The direct contact heat transfer increases with the vapor mass flux as a result of the increased initial transverse velocities imparted upon the droplets by the increased turbulence in the flow. For a wall superheat of 500 K, the delayed onset of direct contact heat transfer with respect to the increasing vapor mass flux is expected. Additionally, the increased heat transfer predicted by the Bajorek-Young model compared to the current model is also a result of the large temperature difference limitation previously discussed and illustrated in Figure 3.

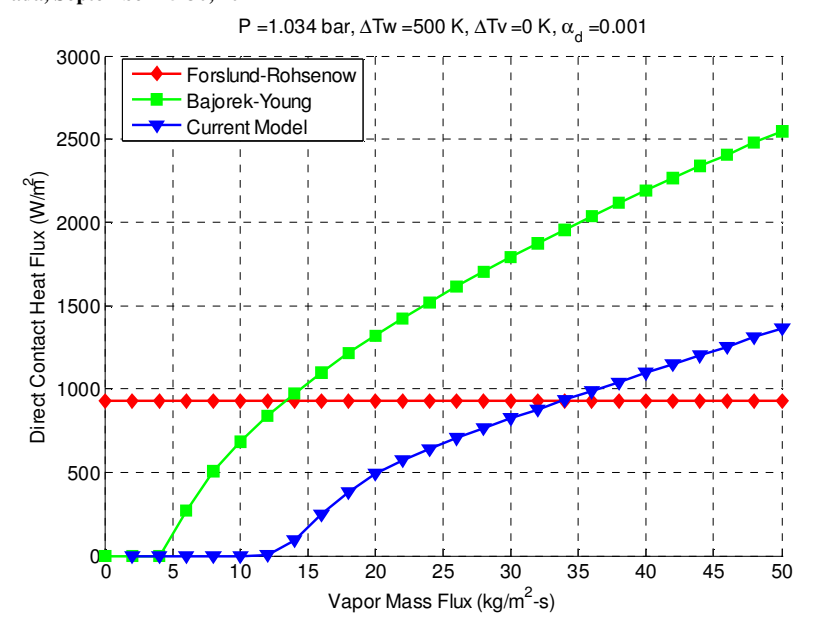


Figure 4: Comparison of Direct Contact Heat Transfer Models for Various Mass Fluxes

5. Conclusions and Future Work

A first principles approach was used to develop a mechanistic model describing the droplet behavior during the process of direct contact heat transfer that can readily be implemented into nuclear reactor safety analysis codes. A two-dimensional force balance is conducted on characteristic droplets to determine if direct contact is possible with the heated wall. If contact is possible, the number of droplets incident on the wall is found to determine the direct contact heat transfer contribution.

In comparison with the previous models, the current model has several advantages. First, the true physics of the situation are modeled explicitly. Second, the new model is applicable over a wide range of conditions and could be applied to numerous fluids. Finally, the current model is directly dependent upon the local conditions (i.e., vapor mass flux, wall superheat, vapor superheat, pressure) and correctly accounts for the physics of direct contact heat transfer taking place in the wall region. Overall, the new model physically models direct contact heat transfer and predicts direct contact heat transfer when contact is possible which is an improvement over previous models. Future work includes mechanistic modeling of the remaining DFFB heat transfer mechanisms to complete a modeling package. The new DFFB heat transfer model will be implemented into a safety analysis code, such as COBRA-TF, for comparison to existing integral experimental data.

6. Acknowledgments

This work was performed under appointment to the Rickover Fellowship Program sponsored by the Office of Naval Reactors of the United States Department of Energy.

7. Nomenclature

- a Droplet diameter [m]
- C_D Drag coefficient [-]
- C_p Specific heat at constant pressure [J/kg-K]
- F_{DE} Differential evaporation force [N]
- f Cumulative deposition factor [-]
- G Mass flux [kg/m²-s]
- g Gravitational constant [9.81 m/s²]
- H_{fg} Latent heat of vaporization [J/kg]
- H_{fg}^* Modified latent heat of vaporization $\left(=H_{fg}+C_{p,v}(T_v-T_{sat})\right)$ [J/kg]
- h Heat transfer coefficient $[W/m^2-K]$
- K_1 Arbitrary constant [-]
- K_2 Correction factor [-]
- *k* Thermal conductivity [W/m-K]
- \dot{m}_d Droplet mass deposition flux [kg/m²-s]
- P(a) Droplet size distribution [m⁻¹]
- q'' Heat flux [W/m²]
- T Temperature [K]
- T_{sat} Saturation temperature [K]
- t Time [s]
- t_R Residence time [s]
- Δt Time step size [s]
- U Local axial vapor velocity [m/s]
- u^* Axial shear velocity [m/s]
- u_0 Initial axial droplet velocity [m/s]
- V Velocity [m/s]
- v_0 Initial transverse droplet velocity [m/s]
- X_A Actual quality [-]
- x Axial location [m]
- y Transverse location [m]
- y^+ Non-dimensional distance from the wall [-]
- Cross-sectional area averaged quantity

Subscripts

- d Droplet
- dc Direct contact
- *l* Liquid phase*t* Tube
- v Vapor phase
- w Wall (heated surface)
- wd Wall to droplet

Superscripts

- Evaluated at the film temperature
- Average (mean) value

Greek Letters

- α_{v} Vapor volume fraction [-]
- μ Dynamic viscosity [Pa-s]
- σ Surface tension [Pa m]
- v Kinematic viscosity $(= \mu / \rho)$ [m²/s]
- ρ Density [kg/m³]

Dimensionless Parameters

$$Nu_L \equiv \frac{hL}{k}$$

$$\Pr \equiv \frac{\mu C_p}{k}$$

$$Re_L \equiv \frac{\rho VL}{\mu}$$

8. References

- [1] Laverty, W.F., and Rohsenow, W.M.: "Dispersed Flow Film Boiling," Journal of Heat Transfer, Vol. 90, 1968, pp. 399-407.
- [2] Baumeister, K.J., Hamill, T.D., and Schoessow, G.J.: "Film Boiling Heat Transfer to Water Drops on a Flat Plate," Chemical Engineering Progress Symposium Series, Vol. 62, Issue 64, 1966, pp. 52-61.
- [3] Iloeje, O.C., Rohsenow, W.M., Griffith, P.: "Three-Step Model of Dispersed Flow Heat Transfer," ASME Heat Transfer Division, 75-WA/HT-1, 1975, 10p.
- [4] Ganic, E.N. and Rohsenow, W.M.: "On the Mechanism of Liquid Drop deposition in Two-Phase Flow," Journal of Heat Transfer, Vol. 101, 1979, pp. 288-294.
- [5] Moose, R.A. and Ganic, E.N.: "On the Calculation of Wall Temperatures in the Post Dryout Heat Transfer Region," International Journal of Multiphase Flow, Vol. 8, No. 5, 1982, pp. 525-542.
- [6] Andreani, M. and Yadigaroglu, G.: "A 3-D Eulerian-Lagrangian Model of Dispersed Flow Film Boiling Including a Mechanistic Description of the Droplet Spectrum Evolution I. The Thermal Hydarulic Model," International Journal of Heat Mass Transfer, Vol. 40, No. 8, 1997, pp.1753-1772.
- [7] Guo, Y. and Mishima, K.: "A Non-Equilibrium Mechanistic Heat Transfer Model for Post-Dryout Dispersed Flow Regime," Experimental Thermal and Fluid Science, Vol. 26, 2002, pp. 861-869.
- [8] Lane, J.W., Hochreiter, L.E., and Aumiller, Jr., D.L.: "Critical Review of The Dispersed Flow Film Boiling (DFFB) Heat Transfer Model Suggested by Forslund and Rohsenow," NURETH-12, Log Number 232, 2007.
- [9] Bajorek, S.M. and Young, M.Y.: "Direct-Contact Heat Transfer Model for Dispersed Flow Film Boiling," Nuclear Technology, Vol. 132, 2000, pp. 375-386.
- [10] Yang, Z.H. and Lee, S.L.: "On the Droplet Deposition and Mist Supercooling in a Turbulent Channel Flow," Part. Part. Syst. Charact., Vol. 8, 1991, pp. 72-78.
- [11] Lee, R. and Almeans, K.: "Droplet Deposition Above a Quench Front During Reflood," *Transactions of the American Nuclear Society*, Vol. 39, 1982, pp. 787-788.
- [12] Liu, Y.H. and Ilori, T.W.: "On the Theory of Aerosol Deposition in Turbulent Pipe Flow," Particle Technology Laboratory Publication, No. 210, University of Minnesota, 1973.
- [13] Schlichting, H.: <u>Boundary Layer Theory</u>, 7th ed., McGraw-Hill (1979).
- [14] Clift, R., Grace, J.R., and Weber, M.E.: <u>Bubbles, Drops, and Particles</u>, Academic Press, 1978.
- [15] Beard, K.V. and Pruppacher, H.R.: "A Wind Tunnel Investigation of the Rate of Evaporation of Small Water Drops Falling at Terminal Velocity in Air," Journal of Atmospheric Science, Vol. 28, 1971, pp. 1445-1464.
- [16] Bolle, L., Moureau, J.C., Spray Cooling of Hot Surface, in: Hewitt, G.F., Delhaye, J.M., Zuber, N., <u>Multiphase Science and Technology</u>, Vol. 1, Hemisphere Publishing, 1986.